Journal of Controlled Release, 26 (1993) 99–108
© 1993 Elsevier Science Publishers B.V. All rights reserved 0168-3659/93/$06.00

COREL 00863

Evidence of mucoadhesion by chain interpenetration at a poly(acrylic acid)/mucin interface using ATR-FTIR spectroscopy

Esmaiel Jabbari, Natalie Wisniewski and Nikolaos A. Peppas

School of Chemical Engineering, Purdue University, West Lafayette, IN 47907-1283, USA

(Received 16 February 1993; accepted in revised form 31 March 1993)

Poly(acrylic acid) is considered to be an important mucoadhesive for controlled release applications. Yet, the specific mechanisms responsible for its bioadhesive behavior are not well understood. Attenuated total reflection infrared spectroscopy (ATR-FTIR) was developed for investigation of chain interpenetration at a poly(acrylic acid) (PAA) and mucin interface. A thin film of acrylic acid, polymerized below the gelation point, was cross-linked directly on an ATR crystal. The cross-linked PAA film was contacted with a buffered mucin solution and the ATR-FTIR spectrum was collected in situ as a function of time. The experimental results show evidence in support of chain interpenetration at the PAA/mucin interface. The experimental results indicate that as PAA and mucin are compatible in the 5–7 pH range, an important mechanism of mucoadhesion is the swelling of PAA by mucin and adhesion is limited by the extent of chain interpenetration across the biointerface.

Key words: Bioadhesion; Mucoadhesion; Poly(acrylic acid); Mucin; Infrared spectroscopy

Introduction

Bioadhesion describes the interfacial interactions between polymeric materials and biological substrates [1,2]. These include hard tissue applications such as in dentistry for adhesion of sealants to tooth surfaces and adhesion of dentures to gum and soft tissue applications such as in ophthalmology for the attachment of conjunctiva to the lid margin and corneal limbal region and in surgery for wound healing [1,3].

One of the most powerful applications of bioadhesion is in controlled release systems for targeted drug delivery to specific areas of the body [4]. The latter is known also as mucoadhesion as the polymer is in contact with the mucosa. Bioadhesive or mucoadhesive polymers are used to immobilize a drug delivery device on a specific site for targeted release and optimal drug delivery due to intimacy and duration of contact. Mucoadhesive polymers have been developed for buccal, nasal, ocular, vaginal, urinary and oral applications [4,5]. In general, the mucoadhesive polymer comes in intimate contact with the epithelium layer. The epithelial goblet cells secrete mucus.

The principal component of the mucus responsible for its gel-like behavior is the glycoprotein component. The mucin gel dissolves completely in water, indicating that the gel is

Correspondence to: N.A. Peppas, School of Chemical Engineering, Purdue University, West Lafayette, IN 47907-1283, USA.

stabilized by non-covalent interactions between the component glycoprotein molecules [1,6–9]. The mucous gel is held together by either primary (disulfide bonds) or secondary bonds (electrostatic and hydrophobic interactions). The mucous gel can be presented as a highly entangled system of macromolecular chains with physical interactions including electrostatic interactions and hydrogen bonding. Therefore, adhesion at the interface between a bioadhesive polymer and mucous can be described by adhesion at polymer–polymer interfaces.

Theories explaining bioadhesion include electrostatic interaction, adsorption theory, wetting theory and chain interpenetration across the biointerface [1,2,10,11]. Wetting and adsorption play an important role in the initial phase of mucoadhesion. The wetting theory states that the adhesion between two polymer surfaces is improved when the two polymers wet each other.

Prominent among various mechanisms contributing to mucoadhesion is the mechanism of chain interdiffusion, proposed by Voyutskii [12] for polymer–polymer interfaces, which was extended to a gel and mucus interface by Mikos [10,11,13] and Ponchel [14–16]. Figure 1 shows the stages of adhesion between two polymer surfaces brought together. After intimate contact is established segments of the two polymers diffuse

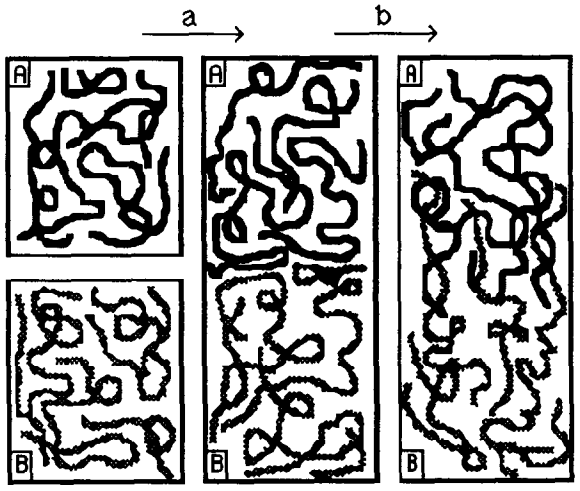

Fig. 1. Stages of polymer/polymer interdiffusion for polymers A and B. a, wetting; b, interdiffusion.

across the interface and the interface heals as a function of time. Therefore, according to this theory, the extent of adhesion at polymer–polymer interfaces is determined by the extent of diffusion and the interfacial thickness between the two polymers.

The major technique for studying bioadhesion has been mechanical testing by fracturing the interface [1,17] usually using a tensiometer. Thus, the fracture theory is used to examine the force necessary to separate the two surfaces after the bioadhesive bond has been established. Robert et al. [18] have used the tensiometric method to measure the bioadhesive strength of different polymers. They report that the most promising bioadhesive substances are anionic polyelectrolytes, particularly cellulosic and acrylic polymers. Sodium alginate showed the highest bioadhesive strength, followed by alginic acid and poly(acrylic acid) (PAA). On the other side, poly(hydroxy ethyl methacrylate) and poly(*N*-vinyl-2-pyrrolidone) showed no adhesive strength. Although tensiometric testing is useful for classification of polymers for mucoadhesion, it is not a very accurate technique and cannot shed light into the mechanisms of adhesion at a biointerface.

Alternatively, Peppas, Duchêne and collaborators [14–16] developed a tensile technique for measurement of the bioadhesive strength of tablets containing PAA in contact with bovine mucus using a tensile tester. Their results showed that the fracture energy increased with increasing PAA content, as previously shown by Park and Robinson [2]. They also observed by electron microscopy that, for the PAA/mucus system, rupture occurred in the mucus layer, whereas in the case of tablets made of pure HPMC, the rupture of the weak adhesive bond seemed to occur at the HPMC/mucus interface. Lehr et al. [19] used electron microscopy to visually examine the interface between cross-linked PAA in contact with mucin. They were unable to observe chain interpenetration at the biointerface due to lack of contrast at low irradiation doses and damage to the interface at high irradiation. These and related studies of Lehr et al.

[20] promoted the idea that chain interpenetration does not occur in polymer/mucus mucoadhesion. To support their results, they commented about the work of Forget et al. [21] who reported measurement of the adhesive forces of various polymers in contact with metallic surfaces. As Forget's data, in their interpretation, are of the same order of magnitude as the mucoadhesive data published by Ponchel et al. [14], they concluded that chain interpenetration is not a mechanism of mucoadhesion as such mechanism would not occur in a polymer in contact with a metallic surface. We believe that Forget's data are not related to bioadhesion and such data should not be compared with the data of Ponchel et al. [14] to disqualify chain interpenetration as a mechanism of mucoadhesion.

To resolve this issue, we concluded that molecular studies could provide additional evidence of chain interpenetration. Here, we present the use of attenuated total reflection infrared spectroscopy, henceforth designated as ATR-FTIR, for spectroscopic investigation of chain interpenetration at a bioadhesive interface consisting of a synthetic polymer such as PAA and mucin. Although a wide variety of spectroscopic techniques have been used to study chain interpenetration at polymer–polymer interfaces [22–27], these techniques have not been used for the investigation of adhesion and interfacial interaction at bioadhesive interfaces consisting of a synthetic polymer and a biological substrate.

Experimental Part

A FTIR spectrometer (Nicolet 800, Madison, WI) with an ATR accessory (Connecticut Instruments, Boston, MA) was used for the interdiffusion studies in the configuration shown in Fig. 2. The ATR crystal was Ge: 5 cm long, 1 cm wide and 2 mm thick. The use of ATR-FTIR for interdiffusion studies at polymer–polymer interfaces is described in detail in reference [26]. In brief, the infrared beam enters the ATR crystal from one of the side faces. If the refractive index of the crystal is higher than the PAA, and the incident angle of the beam is higher than a critical

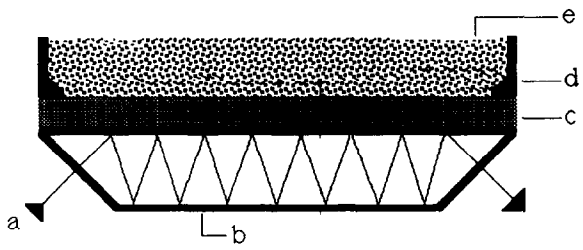

Fig. 2. ATR assembly for in situ measurement of polymer/polymer interdiffusion. a, infrared light beam; b, ATR crystal; c, cross-linked poly(acrylic acid) film; d, sealant to seal off the edges of the crystal; e, mucin solution.

angle, then the infrared beam is totally reflected at the crystal/PAA interface, and the beam travels inside the crystal and exits from the other side face. However, due to diffraction at the crystal surface, a small fraction of the beam penetrates into the PAA layer and is absorbed by PAA. The fraction of the beam which is absorbed gives rise to absorption bands in the ATR spectrum and is used to monitor the concentration of each component within the penetration depth in the polymer layer.

A thin layer of acrylic acid was directly polymerized/cross-linked on the ATR crystal by free radical polymerization. The AA monomer (Aldrich Chemical Co., Milwaukee, WI) was distilled under reduced pressure (5 mmH_g) at 30°C to remove the inhibitor, hydroquinone monomethyl ether. An initiator, 2,2′-azobis-(2methylpropionitrile) (AIBN), and a cross-linking agent, ethylene glycol dimethacrylate (EGDMA) (Aldrich Chemical Co., Milwaukee, WI), were used without further purification.

The following procedure was used for the polymerization. In a reaction flask, 6.85 ml of AA (0.1 mol), 0.0942 ml of EGDMA (0.5 mmol) and 0.009 g of AIBN (0.2 mmol) was mixed with 18 ml of deionized water (1 mol). Initiator was added at 0.5 mol% AIBN per mol AA. The cross-linking ratio used was 0.002 mol EGDMA per mol of AA. The mixture was allowed to react for 3 h at 60°C in a constant temperature bath until the mixture became viscous but before reaching the gelation point. The reaction was stopped by reducing the temperature to 25°C. Thin films of

the reaction mixture was cast on the ATR crystal with a spin coater (model 1-EC101D-485, Photo-Resist Spinners, Garland, TX) at 250 rpm for 2 min. The ATR crystal was transferred to an oven at 70°C for at least 24 h to cross-link the PAA film. The thickness of the PS film was measured using a profilometer (alpha-step 200, Tencor Instruments, Mountain View, CA).

The cross-linked PAA film was dried in vacuo at 25°C for 24 h and contacted with a 1% buffer 7 mucin solution. The buffer 7 solution was prepared by mixing 1.9 ml of a 0.1N citric acid with 8.1 ml of a 0.2 N disodium phosphate aqueous solution. The mucin (Sigma Chemical Co., St. Louis, MO) was extracted from bovine submaxillary glands and was used without further purification. The sides of the ATR crystal were sealed with a sealant to stabilize the mucin solution on the crystal.

To study the effect of pH on the miscibility of PAA and mucin solution, buffered solutions with different pH values were prepared using a mixture of 0.1 N citric acid and 0.2 N disodium phosphate solutions in different proportions. The turbidity of the solution was checked with a UV-VIS spectrophotometer (Model 559, Perkin-Elmer, Indianapolis, IN).

For ATR-FTIR experiments, the spectra were recorded using a Globar (mid-IR) light source with potasium bromide (KBr) as the beam splitter and mercury cadmium telluride (MCT) detector, cooled to liquid nitrogen temperature. The end-face and the optics angle of the beam were 45°. The ATR-FTIR spectrum was collected in situ with 16 averaged scans and a resolution of 4 cm^{-1}.

Results

ATR-FTIR was used to measure chain interpenetration at a bioadhesive interface consisting of cross-linked PAA and mucin. The thickness of the cross-linked PAA film spun on an ATR crystal was measured as a function of distance along the crystal length from the center and is reported in Fig. 3. The cross-linked PAA film thickness was 450 nm.

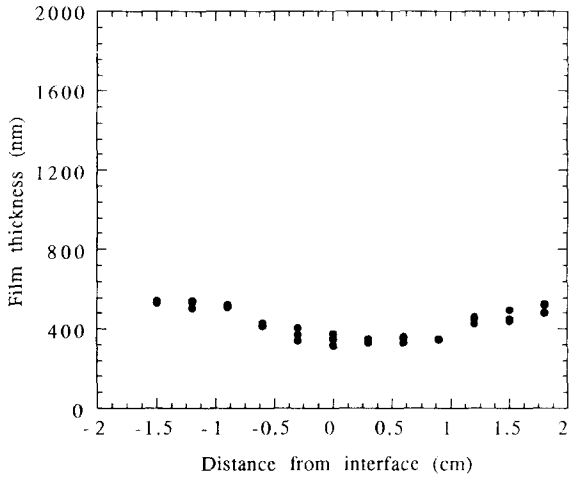

Fig 3. Thickness of the cross-linked poly(acrylic acid) film spin cast on a germanium crystal at 250 rpm for 2 min.

The molecular weight between cross-links, $\bar{M}_c$, was calculated using the Peppas and Lucht model [28] developed for swollen polymer networks, where the cross-links are introduced in the solid state. The equilibrium degree of swelling was 9.3, determined from the relative absorbance of water for cross-linked PAA in contact with buffer 7 aqueous solution (see Fig. 10). The χ factor of 0.45 was used for PAA-water system in buffer 7 aqueous solution [29]. The experimentally determined $\bar{M}_c$ was 7500 g/mol, whereas the theoretical $\bar{M}_c$, calculated from the ratio of cross-linking agent to monomer, was 7200 g/mol resulting in 96% conversion.

As pointed out by Voyutskii [12], the extent of chain interpenetration at a polymer-polymer interface depends on compatibility between the two polymers. For compatible polymers the interface thickness was in the order of microns,whereas for poorly compatible polymers it was in the order of angstroms. The compatibility between PAA and mucin is strongly influenced by the pH of the solution. A citric acid and sodium phosphate buffer was used to study the compatibility of PAA/mucin with pH ranging from 2 to 7. Both PAA and mucin are anionic polyelectrolytes with pK_a of 4.5 and 2.6 [30], respectively.

Table 1 shows the effect of pH on the miscibil-

TABLE 1

Effect of pH on the miscibility of a 2 wt% solution of 50/50 poly(acrylic acid)/mucin solution

pH	Miscibility
2	Immiscible (precipitation)
3	Incompatible (cloudy)
4	Incompatible (cloudy)
5	Compatible (transparent)
6	Compatible (transparent)
7	Compatible (transparent)

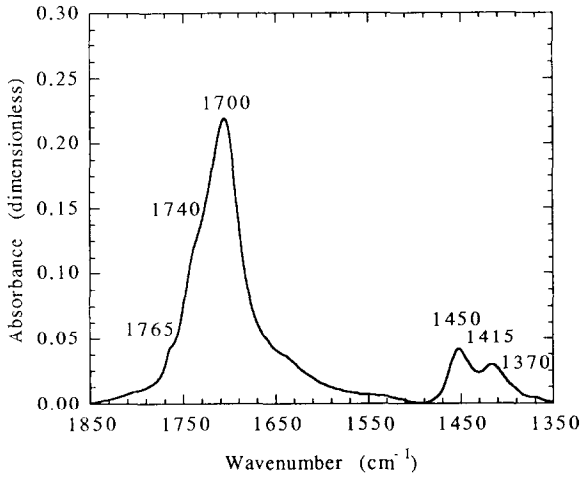

Fig. 4. The ATR-FTIR spectrum of the cross-linked poly(acrylic acid) on germanium crystal.

ity of a 2 wt% solution of 50/50 w/w PAA/mucin solution. The mucin precipitated from the solution with pH 2 indicating that mucin was immiscible with water. Solutions with pH 3 and 4 formed cloudy solutions indicating that they were not compatible with mucin at these pH values. Before the addition of PAA, mucin solutions with pH 5, 6 and 7 were transparent indicating that mucin and water were compatible in these pH values. After the addition of PAA, mucin solutions with pH 5, 6 and 7 were very viscous due to ionization of the carboxylic groups of PAA and mucin and due to hydrogen bonding.

Figure 4 shows the ATR-FTIR spectrum for cross-linked PAA on the ATR crystal in the frequency region from 1350 to 1850 cm^{-1}. The band at 1700 cm^{-1} and the shoulders at 1740 and

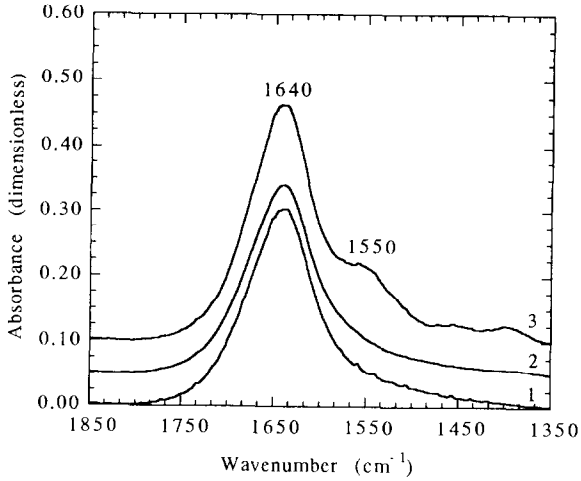

Fig. 5. The ATR-FTIR spectra of deionized water (Curve 1), buffer 7 aqueous solution (Curve 2), and 5% by weight buffer 7 mucin solution (Curve 3).

1765 cm^{-1} are due to carboxylic C=O stretching vibration [31]. The bands with peak locations at 1450, 1415 and 1370 cm^{-1} are the C–O–H bending vibrations of the PAA [31]. The intensity of the these peaks decreases as the PAA is swollen in an aqueous solution.

Figure 5 shows the ATR-FTIR spectrum of deionized water, aqueous buffer 7, and a 5 wt% buffered mucin solution at pH 7. The absorbance scale corresponds to the spectrum of deionized water and the other spectra were shifted by 0.05 absorbance units for visual clarity. The three spectra have one band in common with peak location at 1640 cm^{-1}, which is due to in-plane H–O–H bending vibration [31].

The ATR spectrum of the mucin solution has a band with peak location at 1550 cm^{-1} which is a dimeric C=O stretching vibration [31]. Its intensity is a strong function of composition, as shown in Fig. 6 for a mucin solution of pH 7 at concentrations of 2, 5, 7 and 10 wt%. The mucin peak at 1550 cm^{-1} increases with concentration of mucin.

The following bands were used for quantitative analysis of the PAA/mucin spectrum. The band at 1700 cm^{-1} with shoulders at 1740 and 1765 cm^{-1} was for PAA carboxylic C=O stretching vibration which was proportional to PAA concentration. The band at 1550 cm^{-1} was for

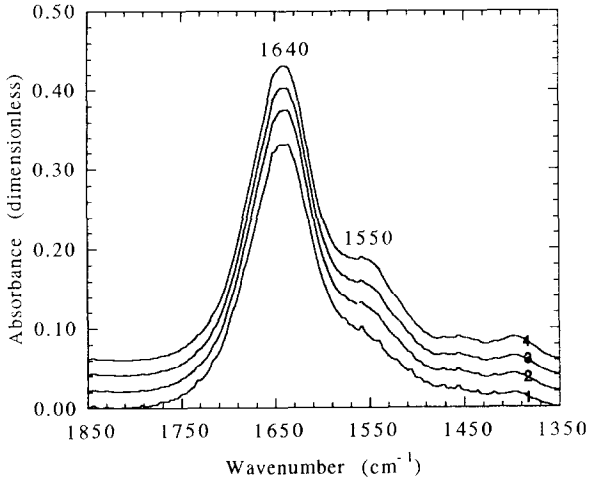

Fig. 6. Composition dependence of the intensity of the mucin band with peak location at 1550 cm^{-1} for 2% (Curve 1), 5% (Curve 2), 7% (Curve 3), and 10% (Curve 4) by weight buffer 7 mucin solution.

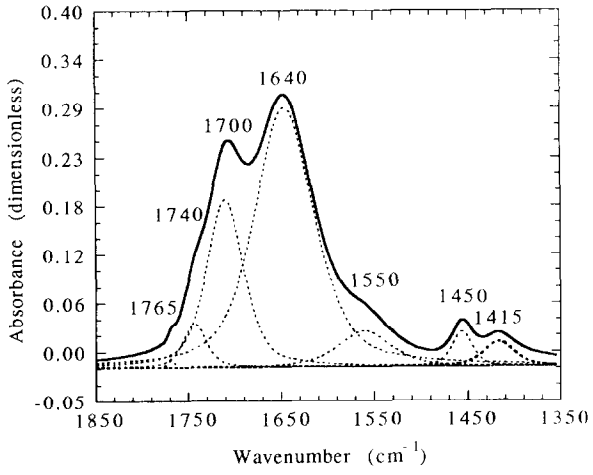

Fig. 7. Deconvolution of ATR-FTIR spectrum for the cross-linked PAA in contact with 1% buffer 7 mucin solution after 360 s of interdiffusion time. The solid line represents the original spectrum, whereas the dashed curves are the deconvoluted peaks using 50% Lorentzian and 50% Gaussian distribution.

mucin dimeric carboxylic C=O stretching, which was proportional to the mucin concentration. The band at 1640 cm^{-1} was for water in-plane H–O–H bending vibration which was proportional to the total concentration of water.

For quantitative analysis, the PAA/mucin

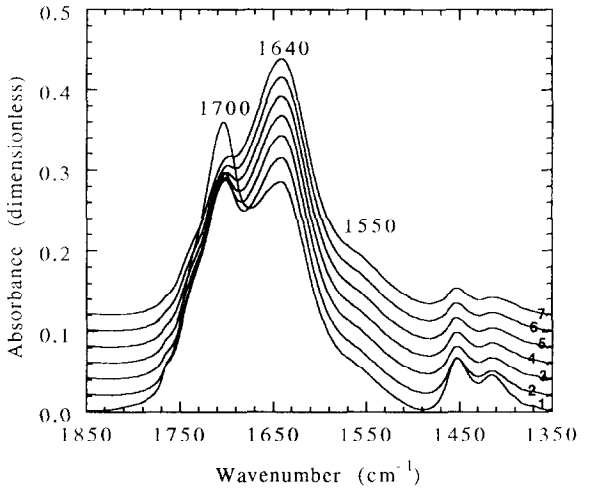

Fig. 8. Time evolution of ATR-FTIR spectra for cross-linked PAA in contact with 1 % buffer 7 mucin solution. The PAA was spin cast from aqueous solution at 250 rpm for 2 min with film thickness of 0.4 μm. The spectra 1 through 7 correspond to 0.0, 2.0, 4.0, 6.0, 8.0, 10.0 and 12.0 min, respectively.

spectra were deconvoluted to relate the area under the peaks to the PAA, mucin, and water concentrations. The deconvolution routine is described elsewhere [26]. Figure 7 shows the actual and the deconvoluted peaks for cross-linked PAA in contact with a 1 wt% mucin solution at pH 7 after 360 s. The best fit was obtained with peaks constructed from a 50% Gaussian and 50% Lorentzian distribution.

Figure 8 shows the time evolution of the ATR-FTIR spectrum for cross-linked PAA film in contact with 1 wt% pH 7 aqueous mucin solution, for a PAA with film thickness of 450 nm. As the water swells the cross-linked PAA film, the intensity of the PAA peak at 1700 cm^{-1} decreases, the intensity of the water peak at 1640 cm^{-1} increases, and the mucin peak at 1550 cm^{-1} shows a slight increase with time. The spectra were deconvoluted and the relative absorbance of PAA, water, and mucin were calculated.

Discussion

The relative intensity of the radiation as a function of distance away from the crystal surface is given by the following equation [32,33]:

$$I_{rel} = e^{-z/d_p} \quad (1)$$

Here, I_{rel} is the initial IR intensity relative to the intensity at the interface, z is the distance from the crystal/PAA interface in the cross-linked PAA layer, and d_p is the penetration depth of IR radiation in the cross-linked PAA layer. According to Eqn. 1, the intensity decreases exponentially away from the interface. The penetration depth of the IR radiation is a function of infrared frequency, refractive index of the crystal and the polymer, and the incident angle of the beam. The penetration depth of the infrared radiation for water and cross-linked PAA on a germanium crystal with incident angle of 45° at 1600 $cm^{-1}$are 200 and 210 nm, respectively, with an average value of 205 nm.

The exponential decrease of IR intensity within the penetration depth has to be considered in order to explain the experimental results shown in Fig 8. For an interdiffusion time, t, the concentration of component i, c_i, at distance z from the crystal surface was multiplied by its corresponding relative intensity, I_{rel}, given by Eqn 1, and it was integrated over the penetration depth of the IR radiation inside the polymer layer. This process was repeated for each interdiffusion time to give the cumulative concentration of component i inside the penetration depth versus time as given by the following equation:

$$Q_i(t) = \frac{\int_0^\infty c_i(z,t) I_{rel}(z)\, dz}{\int_0^\infty I_{rel}(z) dz} \quad (2)$$

Here, component i stands for cross-linked PAA or mucin. Therefore, the experimental results in Fig. 8 are the cumulative concentration of component i inside the penetration depth of infrared beam. For comparison with experimental results, diffusion at the cross-linked PAA/mucin interface is modeled using Fick's law with PAA film thickness of δ_1 and an infinitely thick mucin layer, i.e., the mucin film was at least 50-times thicker than the PAA layer. The diffusion direction is along the z-axis which is perpendicular to the PAA/mucin interface with the origin at the crystal/PAA interface. The differential equation describing the diffusion of component i across the interface as a function of distance and time with a constant diffusion coefficient, D, is given by the following equation:

$$\frac{\partial c_i}{\partial t} = \frac{\partial}{\partial z}\left(D \frac{\partial c_i}{\partial z}\right) \quad (3)$$

The initial and boundary conditions for solving the above diffusion equation are given by the following equations:

$$c_i = 0; \quad 0 \le z \le \delta_1; \quad t = 0 \quad (4)$$

$$c_i = 0; \quad \delta_1 < z \le \infty; \quad t = 0 \quad (5)$$

$$\frac{\partial c_i}{\partial z} = 0; \quad z = 0; \quad t > 0 \quad (6)$$

$$\frac{\partial c_i}{\partial z} = 0; \quad z = \infty; \quad t > 0 \quad (7)$$

The solution to the diffusion Eqn. 3 with the above boundary conditions is given by the following equation [34]:

$$c_i(z,t) = \frac{c_0}{2}\left[\mathrm{erf}\left(\frac{\delta_1 - z}{2\sqrt{Dt}}\right) + \mathrm{erf}\left(\frac{\delta_1 + z}{2\sqrt{Dt}}\right)\right] \quad (8)$$

Here, c_0 is the initial concentration of cross-linked PAA or mucin. Figure 9 compares the model and the experimental results for diffusion of water in cross-linked PAA in contact with buffer 7 aqueous solution. The solid line in Fig. 9 is the best fit to the experimental data with diffusion coefficient of 0.9×10^{-10} 1 cm^2/s and PAA film thickness of 450 nm. The dashed lines above and below the solid line in Fig. 9 are for diffusion coefficient of 1.0×10^{10} and 0.8×10^{-10} cm^2/s, respectively. The diffusion coefficient obtained from the experimental data is in good agreement with the values reported in the literature for diffusion of water in glassy polymers.

Figure 10 compares the time evolution of the relative absorbance of water for PAA in contact with deionized water, a pH 7 aqueous solution, and a 1 wt% pH 7 aqueous mucin solution. The rate of swelling of PAA is highest for buffered solution at pH 7. As mucin is added to the buffered

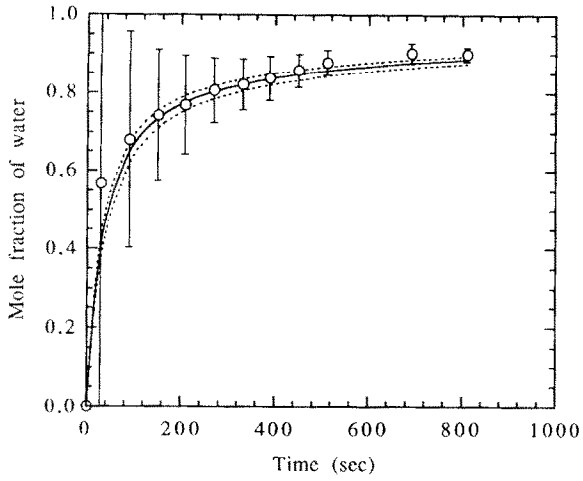

Fig. 9. Comparison of the experimental relative absorbance of water as a function of time (open circles) and the Fickian model with constant constant diffusion coefficient. The solid line is the best fit using Eqns 2 and 8 with diffusion coefficient of 0.9×10^{-10} cm^2/s. The dashed lines above and below the solid line are the Fickian model prediction with diffusion coefficient of 1.0×10^{-10} and 0.8×10^{-10} cm^2/s, respectively. The PAA film thickness was 450 nm.

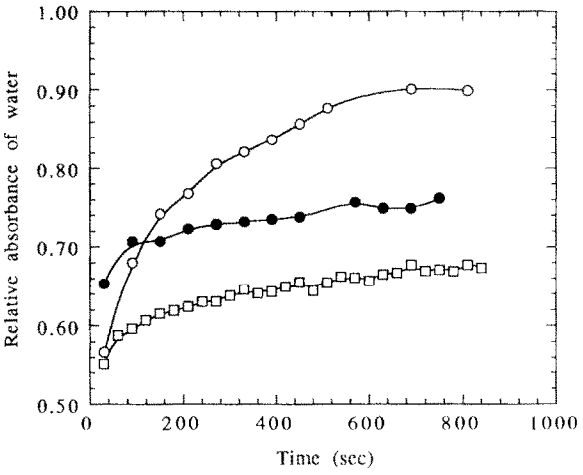

Fig. 10. Relative absorbance of water as a function of time for cross-linked PAA in contact with deionized water (○), buffer 7 aqueous solution (●), and 1% buffer 7 mucin solution (□). The PAA was spin cast from aqueous solution at 250 rpm for 2 min with film thickness of 0.4 μm.

solution at pH 7, the rate of swelling decreases significantly. The rate of swelling of PAA is higher in a buffered solution at pH 7 than in deionized water which is consistent with compatibility and

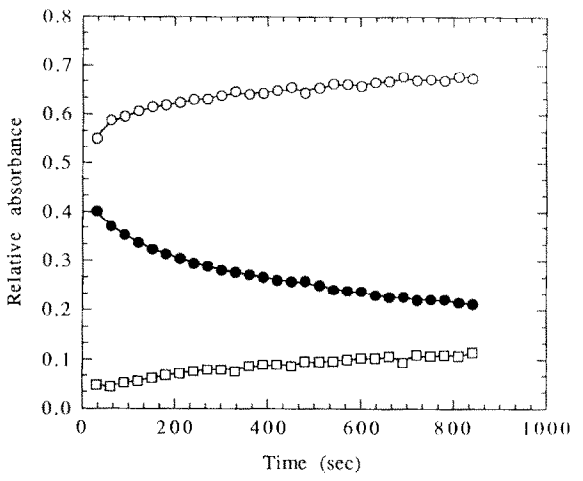

Fig. 11. Relative absorbance of water (○), PAA (●) and mucin (□) as a function of time for cross-linked PAA in contact with 1% buffer 7 mucin solution. The PAA was spin cast from aqueous solution at 250 rpm for 2 min with film thickness of 0.4 μm.

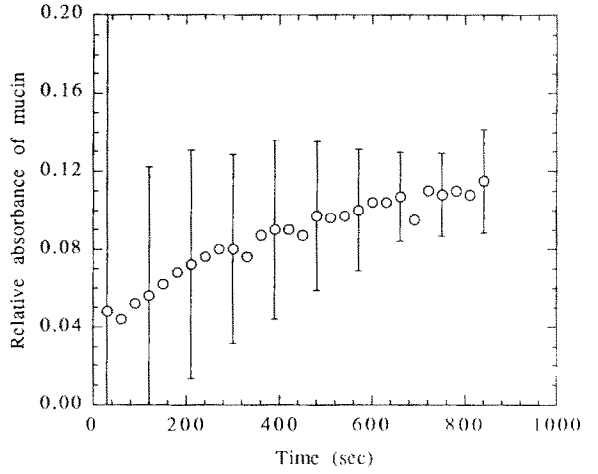

Fig. 12. Relative absorbance of mucin with error bars as a function of time for cross-linked PAA in contact with 1% buffer 7 mucin solution. The PAA was spin cast from aqueous solution at 250 rpm for 2 min with film thickness of 0.4 μm.

phase behavior of PAA and mucin shown in Table 1. The increased rate of swelling of PAA in a buffered solution at pH 7 is due to increase in the degree of ionization of PAA in pH 7 compared to deionized water. Consequently, the mucin solution is more compatible with PAA in a buffered solution at pH 7 than in deionized water as

evidenced by the rate of swelling in Fig. 10.

Figure 11 shows the time evolution of the relative absorbance of PAA, water, and mucin for PAA in contact with a 1 wt% pH 7 mucin solution at 25°C. The relative absorbance of PAA decreases with swelling and the relative absorbance of water and mucin increases indicating that water and mucin swell the PAA matrix simultaneously.

Figure 12 shows the relative absorbance of mucin as a function of time with the corresponding error bars determined from the errors due to intensity and line width of the ATR-FTIR peaks. Although the error bars are large, there is good indication that the concentration of mucin increases with time and mucin and water swell the PAA matrix. The mucin swells the PAA matrix because PAA and mucin are miscible and compatible for pH 7, as indicated in Table 1. These results offer unequivocal proof that chain interdiffusion occurs at PAA/mucin interfaces and support the idea of mucoadhesion due to chain interpenetration.

Conclusions

Results indicate that the compatibility of PAA and mucin is strongly influenced by the pH. The experimental results indicate that mucoadhesion depends on the compatibility of PAA and mucin under specific conditions such as pH or ionic strength. If the PAA and mucin are completely compatible, an important mechanism of mucoadhesion is chain interdiffusion as the mucin swells the cross-linked PAA matrix.

Acknowledgement

This work was supported grant No. GM 45027 from the National Institute of Health.

References

1 N.A. Peppas and P.A. Buri, Surface, interfacial and molecular aspects of polymer bioadhesion on soft tissues, J. Controlled Release 2 (1985) 257.

2 H. Park and J.R. Robinson, Mechanisms of mucoadhesion of poly(acrylic acid) hydrogels, Pharm. Res. 4 (1987) 457-464.

3 R.E. Baier, Cell adhesion to biomedical surfaces: conflicts and concerns J. Biomed. Mater. Res. 16 (1982) 173-186.

4 R. Gurny and H.E. Junginger, Bioadhesion: Possibilities and Future Trends, Wissenschaftliche Verlagsgesellschaft, Stuttgart, 1990.

5 V. Lenaerts and R. Gurny, Eds., Bioadhesive Drug Delivery Systems, CRC Press, Boca Raton, FL, 1990.

6 C. Marriot and D.R.L. Hughes, Mucus physiology and pathology, in Bioadhesion Possibilities and Future Trends, R. Gurny and H.E. Junginger, Eds., pp. 29-43, Wissenschaftliche Verlagsgesellschaft, 1990.

7 N.A. Peppas, P.J. Hansen and P.A. Buri, A theory of molecular diffusion in the intestinal mucus, Intern. J. Pharm. 20 (1984) 107-115.

8 A. Allen, R.H. Pain and T.R. Robson, Model for the structure of the gastric mucous gel, Nature 264 (1976) 88-89.

9 L.M. Reid and J.R. Clamp, The biochemical and histochemical nomenclature of mucus, Br. Med. Bull. 34 (1978) 5-7.

10 A.G. Mikos and N.A. Peppas, Scaling concepts and molecular theories of adhesion of synthetic polymers to glycoproteinic networks, in Bioadhesive Drug Delivery Systems, V. Lenaerts and R. Gurny, Eds., pp. 25-42, CRC Press, Boca Raton, FL, 1990.

11 N.A. Peppas and A.G. Mikos, Kinetics of mucus-polymer interactions, in Bioadhesion: Possibilities and Future Trends, R. Gurny and H.E. Junginger, Eds., pp. 65-85, Wissenschaftliche Verlagsgesellschaft, 1990.

12 S.S. Voyutskii, Some comments on the series of papers "interfacial contact and bonding in autohesion, J. Adhesion (1971) 69-76.

13 A.G. Mikos and N.A. Peppas, Polymer chain entanglements and brittle fracture, J. Chem. Phys. 88 (1988) 1337-1342.

14 G. Ponchel, F. Touchard, D. Duchéne and N.A. Peppas, Bioadhesive analysis of controlled-release systems. I. Fracture and interpenetration analysis in poly(acrylic acid) containing systems, J. Controlled Release 5 (1987) 129-141.

15 N.A. Peppas, G. Ponchel and D. Duchéne, Bioadhesive analysis of controlled-release systems. II. Time-dependent bioadhesive stress in poly(acrylic acid)-containing systems, J. Controlled Release 5 (1987) 143-150.

16 G. Ponchel, F. Touchard, D. Wouessidjewe, D. Duchéne and N.A. Peppas, Bioadhesive analysis of controlled-release systems. III. Bioadhesive and release behavior of metroindazole-containing poly(acrylic acid)-hydroxy propyl methyl cellulose systems, Int. J. Pharm. 38 (1987) 65-69.

17 K. Park and H. Park, Test methods of bioadhesion, in Bioadhesive Drug Delivery Systems, V. Lenaerts and R. Gurny, Eds., pp. 43-64, CRC Press, Boca Raton, FL, 1990.

18 C. Robert, P. Buri and N.A. Peppas, Experimental method for bioadhesive testing of various polymers, Acta. Pharm. Technol. 2 (1988) 95-98.
19 C.-M. Lehr, J.A. Bouwstra, F. Spies, J. Onderwater, J. van het Noordeinde, C. Vermeij-Keers, C.J. van Munsteren, and H.E. Junginger, Visualization studies of the mucoadhesive interface, J. Controlled Release 18 (1992) 249-260.
20 C.M. Lehr, J.A. Bouwstra, H.E. Bodde and H.E. Junginger, A surface energy analysis of mucoadhesion: contact angle measurements on polycarbophil and pig intestinal mucosa in physiologically relevant fluids, Pharm. Res. 9 (1992) 70-75.
21 P. Forget, P. Gazzeri, F. Moreau, M. Sabatier, C. Durandeau, J.P. Merlet and P. Aumonier, Comprimé mucoadhesifs: mesure de l'adhesivité in vitro, S.T.P. Pharma. 4 (1988) 176-181.
22 A. Karim, G.P. Felcher and T.P. Russell, Diffusion studies in polymer bilayers by neutron reflection, Polym. Prepr. 31(2) (1990) 69-70.
23 C.M. Roland and G.G.A. Bohm, Molecular diffusion and the autoadhesion of polybutadiene, Macromolecules 18 (1985) 1310-1314.
24 J. Klein and B.J. Briscoe, Diffusion of large molecules in polymers: a measuring technique based on microdensitometry in the infra-red, Polymer 17 (1976) 481-484.
25 E. Jabbari and N.A. Peppas, Mapping the concentration profile at the poly(vinylchloride) and poly(ethyl methacrylate) interface, Polym. Bull. 7 (1991) 305-309.
26 E. Jabbari and N.A. Peppas, The use of ATR-FTIR to study interdiffusion in polystyrene and poly(vinyl methyl ether), Macromolecules, 26 (1993) 2175–2186.
27 N.A.B.B. Sauer and D.J. Walsh, The use of neutron reflection and spectroscopic ellipsometry for the study of the interface between miscible polymer films, Macromolecules 24 (1991) 5948-5956.
28 N.A. Peppas (Ed.), Hydrogels in Medicine and Pharmacy. I. Fundamentals, CRC Press, Boca Raton, FL, 1986, p. 36.
29 A.F.M. Barton, Handbook of Polymer-Liquid Interaction Parameters, CRC Press, Boca Raton, FL, 1990.
30 P.M. Johnson and K.D. Rainsford, The physical properties of mucus: preliminary observations on the sedimentation behavior of porcine gastric mucus, Biochim. Biophys. Acta 286 (1972) 72-84.
31 R.M. Silverstein, G.C. Bassler and T.C. Morrill, Spectroscopic Identification of Organic Compounds, p. 120, Wiley, New York, 1981.
32 N.J. Harrick, Internal Reflection Spectroscopy, p. 27, Wiley, New York, 1967.
33 K. Knutson and D.J. Lyman, in Biomaterials: Interfacial Phenomena and Applications, Advances in Chemistry Series, Vol. 199, p. 197, American Chemical Society, Washington, DC, 1982.
34 J. Crank, The Mathematics of Diffusion, p. 16, Clarendon Press, Oxford, London, 1975.